Spectral Broadening of NWC Transmitter Signals in the ionosphere

Zhiyang Xia, Lunjin Chen, Zeren Zhima, Michel Parrot

Geophysical Research Letters

RESEARCH LETTER
10.1029/2020GL088103

Spectral Broadening of NWC Transmitter Signals in the Ionosphere

Zhiyang Xia[1], Lunjin Chen[1], Zeren Zhima[2], and Michel Parrot[3]

[1]Department of Physics, University of Texas at Dallas, Richardson, TX, USA, [2]Institute of Crustal Dynamics, China Earthquake Administration, Beijing, China, [3]LPC2E/CNRS, Orléans, France

Key Points:

- The broadened emissions are electrostatic and occur at both hemispheres, in both VLF and HF frequency bands at nightside
- The intensity and frequency width of the broadened VLF spectra increase as the NWC amplitude increases
- The intensity and frequency width of the broadened VLF spectra increase as the background electron density decreases

Correspondence to:
Z. Xia and L. Chen,
Zhiyang.Xia@utdallas.edu;
lunjin.chen@gmail.com

Citation:
Xia, Z., Chen, L., Zhima, Z., & Parrot, M. (2020). Spectral broadening of NWC transmitter signals in the ionosphere. *Geophysical Research Letters*, *47*, e2020GL088103. https://doi.org/10.1029/2020GL088103

Received 24 MAR 2020
Accepted 18 MAY 2020
Accepted article online 30 MAY 2020

Abstract In this study, we use about 6.5 years of observation of Detection of Electromagnetic Emissions Transmitted from Earthquake Regions (DEMETER) satellite to study the spectral broadening of NWC ground transmitter signals and examine key parameters that control the width and intensity of the broadening power. First, we analyze a typical spectral broadening event, with enhanced wave intensity between lower hybrid resonance frequency and NWC signal frequency (19.8 kHz). The width and intensity of broadening power are positively proportional to the NWC wave amplitude. A following statistical analysis reveals a similar dependence on the NWC wave amplitude. The statistical analysis also indicates a significantly negative correlation of broadening spectral intensity and width with the background plasma density. The observations are consistent with existing theories predicting that lower plasma density drives a lower threshold for spectral broadening.

1. Introduction

Very low frequency (VLF) waves emitted by ground-based transmitters can penetrate through the ionosphere into the plasmasphere and cause ionospheric perturbations, particle precipitation, and heating (Bell et al., 2011; Gamble et al., 2008; Graf et al., 2009; Inan et al., 2007; Li et al., 2012; Marshall et al., 2010; Parrot et al., 2007, 2009; Sauvaud et al., 2008). Energetic electrons can interact with VLF waves through the cyclotron resonance and lower hybrid parametric instabilities which may be produced by VLF transmitters (Riggin & Kelley, 1982). Parrot et al. (2007) reported an event which observed plasma perturbations caused by VLF emissions from the NWC transmitter. The NWC transmitter, located in Australia, operates with a frequency of 19.8 kHz and has very strong emission power (1,000 kW), which can cause significant perturbations of electron density and temperature, as well as heating of ions in the ionosphere. Accompanied with these ionospheric perturbations, broadband electrostatic emissions from lower hybrid frequency (f_{lhr}) to 19.8 kHz (VLF band) and from upper hybrid frequency (f_{uhr}) to about 2.5 MHz (medium frequency [MF] band) were also observed. It has been suggested that the enhanced MF band electrostatic waves are caused by the lightning-generated whistler waves that penetrate through the ionosphere due to the electron density perturbations caused by the VLF transmitter (Parrot et al., 2009). Mishin et al. (2010) investigated potential plasma instabilities leading to the broadband VLF emissions and concluded that the energy loss of the VLF signals and the excitation of broadband VLF emissions are caused by nonlinear interactions based on the event of Parrot et al. (2007). Later, Galinsky et al. (2011) used a 3-D numerical model to simulate the nonlinear interactions of lower hybrid waves and reproduced the broadband lower hybrid electrostatic emissions that were observed by the Detection of Electromagnetic Emissions Transmitted from Earthquake Regions (DEMETER) satellite in Parrot et al. (2007). It should be noted that, besides the NWC transmitter signal, lightning-generated whistlers can also generate lower-hybrid turbulence, which can be observed in middle and low latitude regions (Berthelier et al., 2008).

In this study, we use about 6 years of observations of DEMETER satellite to analyze the spectral broadening phenomenon of the NWC VLF transmitter emission in the ionosphere. Different payloads on DEMETER provide the measurements of the wave power spectra in both VLF and high frequency (HF) bands as well as the variations of plasma density and temperature, which are suitable for this study. We aim at determining where the spectral broadening occurs. Moreover, we also check the dependence of the intensity and frequency width of the broadband emission on background parameters including the intensity of the NWC transmitter, the background magnetic field, plasma density, and electron temperature. In section 2, we give a brief introduction of the DEMETER satellite and its instruments. In section 3, the statistical results of the

spectral broadening are shown. Finally, we provide the background parameter dependence analysis of the spectral broadening in section 4.

2. Spacecraft and Instruments

DEMETER is a French satellite with a low-altitude nearly Sun-synchronous circular orbit (~10:30 and ~22:30 LT). It was operated over a ~6.5-year period from June 2004 to December 2010. The altitude of the spacecraft was initially 710 km before December 2005 and then decreased to 660 km (Parrot et al., 2006). The Instrument Champ Electrique (ICE) (Berthelier et al., 2006b) onboard consists of four sensors, which are spherical aluminum electrodes with a 60-mm diameter and deployed by stacer booms at approximately 4 m from the satellite. It can provide measurements of the electric field in the frequency range from DC/ULF band (0–15 Hz) up to HF band (10 kHz to 3.175 MHz). The Instrument Magnetic Search Coil (IMSC) (Parrot et al., 2006) can provide the measurement of the magnetic field from a few Hz to 20 kHz. The Instrument Sonde de Langmuir (ISL) is a Langmuir probe that can measure the density and temperature of electrons (Lebreton et al., 2006). The Instrument Analyseur de Plasma (IAP) is a two-analyzer spectrometer that measures the ion density, composition, temperature, and flow velocity (Berthelier et al., 2006a). The background magnetic field data are calculated from the International Geomagnetic Reference Field (IGRF) model.

3. Observations of Spectral Broadening

Figure 1 shows an event of NWC transmitter signal spectral broadening observed by the DEMETER satellite on 2 June 2006 at nightside (with magnetic local time [MLT] around 22.3), which shows similar features as those in the event reported by Parrot et al. (2007). This event lasts about 4 min from ~14:50:30 UT to ~14:54:30 UT, during which the DEMETER was flying over the NWC ground transmitter. Figures 1a–1e show the electric wave power spectra density (P) of HF and VLF frequency bands, the electron density, the electron temperature, and the ion temperature, respectively. One can see enhanced emissions of broadband spectra in both HF and VLF frequency bands during this time interval. The enhanced HF band emission is confined above the upper hybrid frequency (f_{UHR}) while the enhanced VLF band emission is confined between the lower hybrid frequency (f_{LHR}) and the NWC transmitter signal frequency (19.8 kHz). Coincident with the enhanced emissions, there are pronounced disturbances in the electron density and temperature (Figures 1c–1d) and elevated ion temperature (Figure 1e). It should be noted that NWC transmitter signals that are also detected beyond the 3-min period of the spectral broadening event do not present the spectral broadening signatures. We replot the VLF power spectral density (Figure 1b) sorted by NWC transmitter wave electric field amplitude (A_{NWC}) in Figure 1f. A_{NWC} is calculated by $\sqrt{\sum_{f_i} P(f_i)\Delta f}$, where 21 frequency channels f_i in the range from 19.609 to 20 kHz are used, $P(f_i)$ is the wave power spectral density at the frequency channel f_i, and Δf is the frequency channel width (~19.53 Hz) of the observed VLF spectra. One can see that only a certain subset of NWC transmitter signals of sufficient amplitude (about a critical value of $10^{3.4}\mu$V/m) is capable of triggering the broadening spectra in the VLF band. For those signals of sufficient amplitudes, both the intensity and frequency width of the broadband VLF emission increase as A_{NWC} increases.

To reveal the statistical characteristics of NWC transmitter spectral broadening occurrence, we make use of about 6 years (the mission time of DEMETER is about 6.5 years, but we exclude the period from June 2007 to Jan 2008 since the NWC transmitter was turned off in this period) of wave and plasma observations from the DEMETER satellite, with an emphasis at nightside (since NWC signals at dayside are much weaker (Zhang et al., 2018) and thus less likely to cause spectral broadening). Figures 2a and 2b show the spatial distribution (in geomagnetic latitude and longitude) of the geometric mean electric wave intensity measured by DEMETER satellite at nightside for two selected frequency channels, 19.805 kHz (which is the closest frequency to the NWC signal frequency) and 15 kHz, respectively. The widths for geomagnetic longitude and latitude bins are both 1°. From the 19.805 kHz map (Figure 2a), one can see two broad regions (of longitudinal and latitudinal widths over 15°) with strongly enhanced emissions from the NWC transmitter, one centered around the NWC transmitter in the southern hemisphere and the other one near its conjugate point in the northern hemisphere. The peaks of these two strong emission regions are marked by the two magenta open circles. For the map of 15 kHz (Figure 2b), there is considerable wave spectral power density above the background emission near the corresponding peaks

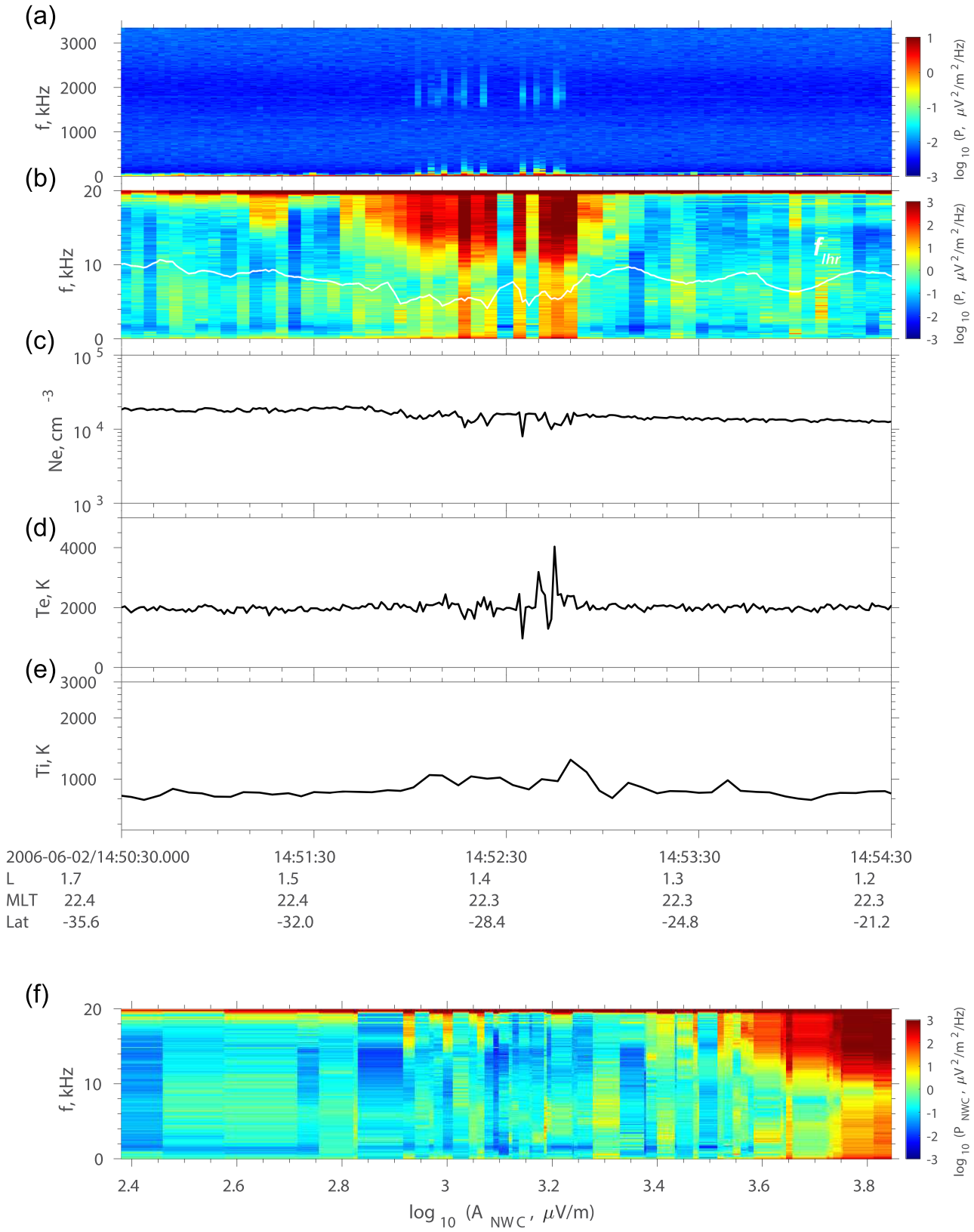

Figure 1. Overview of the spectral broadening event. (a) The electric wave power spectra in the HF band; (b) the electric wave power spectra in the VLF band; (c) the variation of electron density; (d) the variation of electron temperature; (e) the variation of ion temperature; (f) the VLF power spectra as a function of the amplitude of NWC signal. The white solid line in panel (b) denotes the lower hybrid resonance frequency.

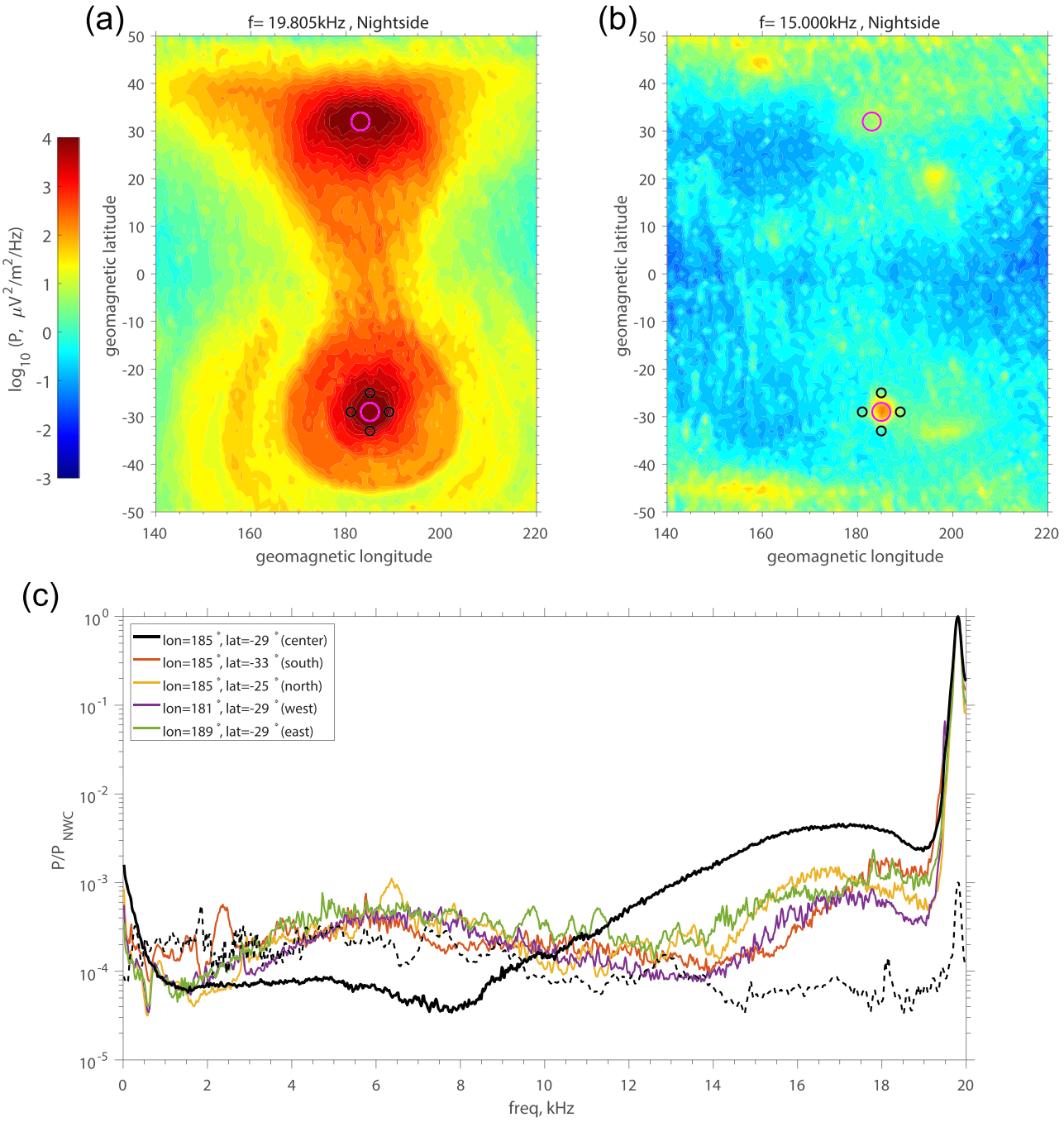

Figure 2. The mean electric field intensity spatial distribution in geomagnetic longitude (*x*-axis) and latitude (*y*-axis) at nightside for (a) 19.805 kHz and (b) 15 kHz. The magenta open circles mark the location of maximum NWC signal wave intensity in the southern and northern hemispheres. (c) The electric wave intensity variation versus wave frequency at five selected locations: the center point with the maximum wave power over the NWC transmitter (the magenta circles in the southern hemisphere in panels (a) and (b)) and the other four location bins 4° east, west, south, and north from the center point. The black dashed line represents the spectrum at a location significantly far from (60° west of) the central point.

at 19.8 kHz (marked by the two open magenta circles), although much weaker than that at the frequency channel of 19.8 kHz. Figure 2c shows the comparison of broadened spectra at the southern hemisphere peak and four other location bins nearby (marked by the four open black circles in Figures 2a and 2b), corresponding to locations 4° southward, northward, westward, and eastward of the peak point. In

Figure 2c, the values of the geometric mean of the electric wave power spectral density are normalized by the value at the frequency channel of 19.8 kHz (NWC signal frequency) to highlight the variation of the frequency range of the broadened spectra. Among the five power spectral curves, there are common peaks at the NWC transmitter operation frequency (19.8 kHz), which sharply fall off till the upper frequency limit of the ICE instrument (20 kHz) and down to ~19 kHz. There exists another enhanced emission over the frequency range from ~10 to ~19 kHz, which is more pronounced for the spectrum at the center point (denoted by the black line in Figure 2c) than the other four locations. The four colored lines show similar variations since the transmitter distributed symmetrically around the center point, and the intensity from ~10 to ~19 kHz of the colored lines are much weaker than that of the black line. It should be noted that the absolute wave intensity near 19.8 kHz at the four location bins of the colored lines are much weaker than that of the center point (the black solid line), meaning that the absolute intensity of broadening waves at the four locations corresponding to the colored lines should be even weaker than that of the center point. The VLF wave broadening spectra preferentially occur at the location of stronger NWC transmitter signals. The broadened spectra occur over a broader frequency range below the NWC operation frequency, from ~10 to ~19 kHz at the center point, while over a relatively narrow frequency range at the other four locations, from ~14 to ~19 kHz. It is also shown that there exists a secondary enhancement over the frequency range of 2–10 kHz, which is more pronounced at the four locations away from the center. To check whether this enhancement corresponds to NWC signal, we add a control line (the black dashed line), which is obtained by the mean wave intensity at a location significantly away from the NWC signal peak (60° westward of the center point as an example, normalized by the same NWC intensity of the purple line). We find a similar secondary enhancement in the control line. Thus, this enhancement should not relate to the NWC signals and may be caused by the presence of the natural background wave power.

The spectral broadening of the NWC transmitter reported above occurs at nightside for electric wave intensity in the VLF frequency range near both the NWC transmitter location (southern hemisphere) and its conjugate point (northern hemisphere). We also perform a similar analysis on the VLF wave magnetic field spectra (IMSC instrument) and at dayside. We find that significant spectral broadening can be observed only at nightside rather than at dayside and for the electric rather than magnetic wave spectra. We should note that the spectral broadening of the HF frequency band is much more significant near the NWC location in the southern hemisphere than the northern hemisphere (not shown), which is consistent with Parrot et al. (2009).

4. Preferred Conditions for Spectral Broadening

As shown above, not all NWC transmitter signals are accompanied with the spectral broadening phenomena, and when they occur, the broadened spectra show varying spectral width and varying intensity. Based on DEMETER wave and particle measurements over its mission life (~6.5 years), we investigate the preferred conditions of the spectral broadening phenomena and the dependence of broadened spectra on background parameters. The background parameters we checked include the amplitude of NWC transmitter signals, the background magnetic field, the electron density, and the electron temperature. We examine VLF wave electric field spectra at the location bins within 10° in geomagnetic longitude and within 5° in geomagnetic latitude of the center points of peak NWC signal intensity in the southern and northern hemispheres. We select the VLF spectra with the presence of NWC transmitter signals only, which is identified by the criterion that the power spectral density at 19.805 kHz is at least one order of magnitude larger than those at two neighboring frequency channels (at 20 and 19.609 kHz). Then we sort the selected spectra into the bins of NWC amplitude A_{NWC} and evaluate the geometric averages of the spectra in each bin for northern hemisphere (Figure 3a) and southern hemisphere (Figure 3c), respectively. Figures 3b and 3d show the corresponding numbers of the spectra in each bin. Similar to the event observation shown in Figure 1, the intensity and width of the broadened spectra increase as the NWC amplitude increases. The threshold value of the NWC amplitude to form the broadened spectra is about $10^{3.4}\mu$V/m.

In order to isolate the dependence of spectral broadening on the electron density (measured by the ISL instrument) from the dependence on NWC wave amplitude, we select the VLF spectra with the additional

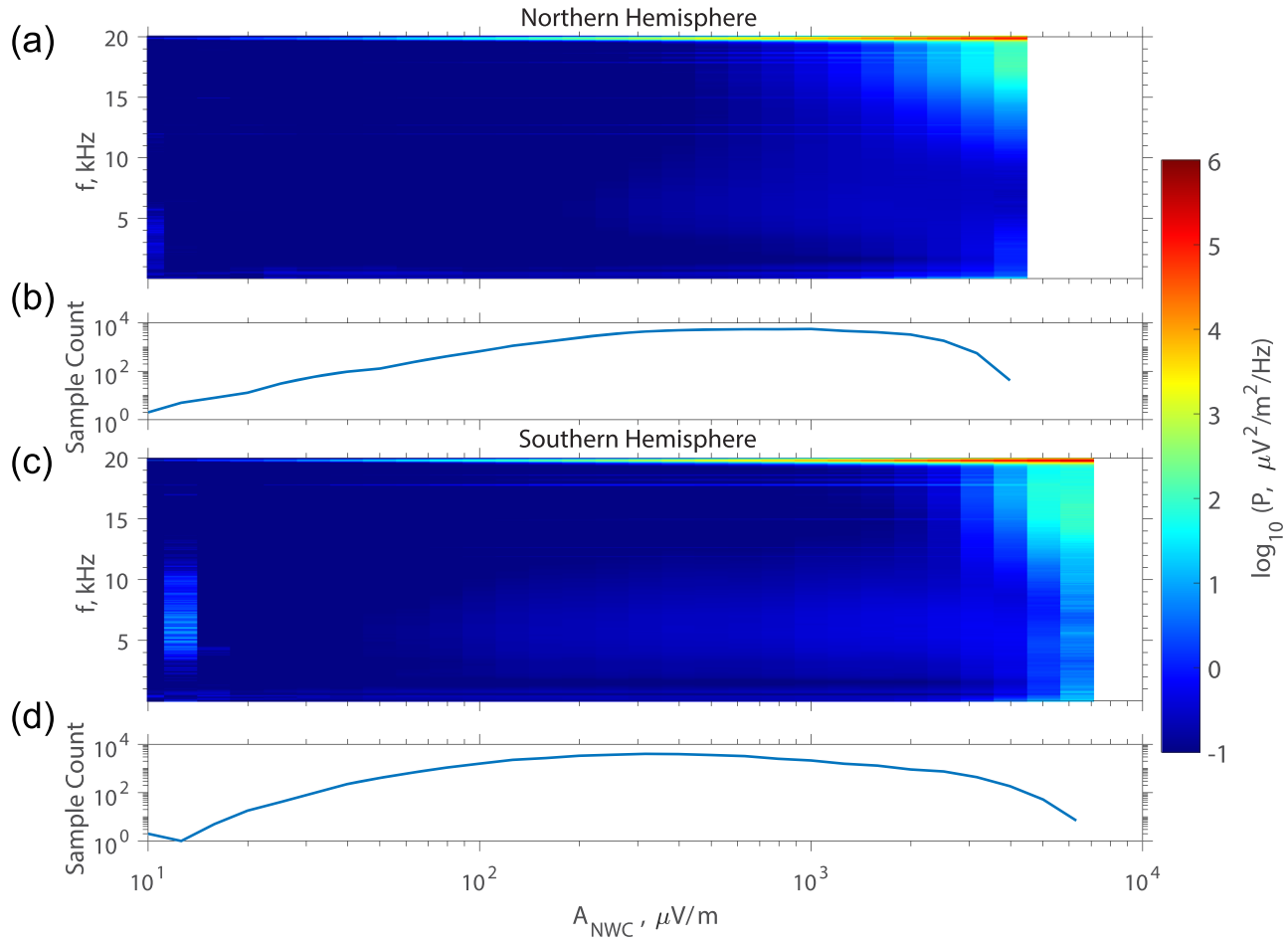

Figure 3. (a) and (c) are the VLF electric wave power spectra versus frequency (y-axis) and NWC amplitude (x-axis) at nightside in the northern and southern hemispheres, respectively. (b) and (d) are the corresponding numbers of spectra in each NWC amplitude bins.

constraint of NWC wave amplitude A_{NWC} in a narrow range from $10^{3.5}$ to $10^{3.6}$ μV/m and then sort the spectra into bins of the electron density. The effect of plasma density is shown in Figure 4. Figures 4a and 4d are the geometric averages of electric wave spectral density in each bin of electron density in the northern and southern hemispheres, respectively. The corresponding numbers of the VLF spectra in each density bin are shown in Figures 4b and 4e. The corresponding geometric averaged NWC amplitudes, in Figures 4c and 4f, verify that the effect of NWC amplitude has been minimized in this analysis since the averaged NWC amplitudes in each plasma density bin are nearly the same (Figures 4c and 4f). One can see that the intensity and width of the broadened VLF spectra tend to increase as the plasma density decreases (Figures 4a and 4d). Although the absolute value of the electron density measured by the ISL instrument may not be very accurate, the relative change of electron density is of interest here when considering the effect of plasma density on the spectral broadening. We also use a similar analysis to isolate the effects of the other two parameters, the background magnetic field and the electron temperature, and find no significant dependency on them (not shown). This does not mean that the spectral broadening is independent of these two parameters for the following reason. Unlike the significant variation of plasma density in the selected region above the NWC station from the DEMETER observation, the variation of the other two parameters is not large enough to show their effects. The background magnetic field only varies by ~10% in the selected spatial regions, while electron temperature varies only about a factor of ~2 (from 1400 to 3400 K in the southern hemisphere and from 1800 to 3000 K in the northern hemisphere). The small variations make it difficult to isolate the dependencies on the two parameters.

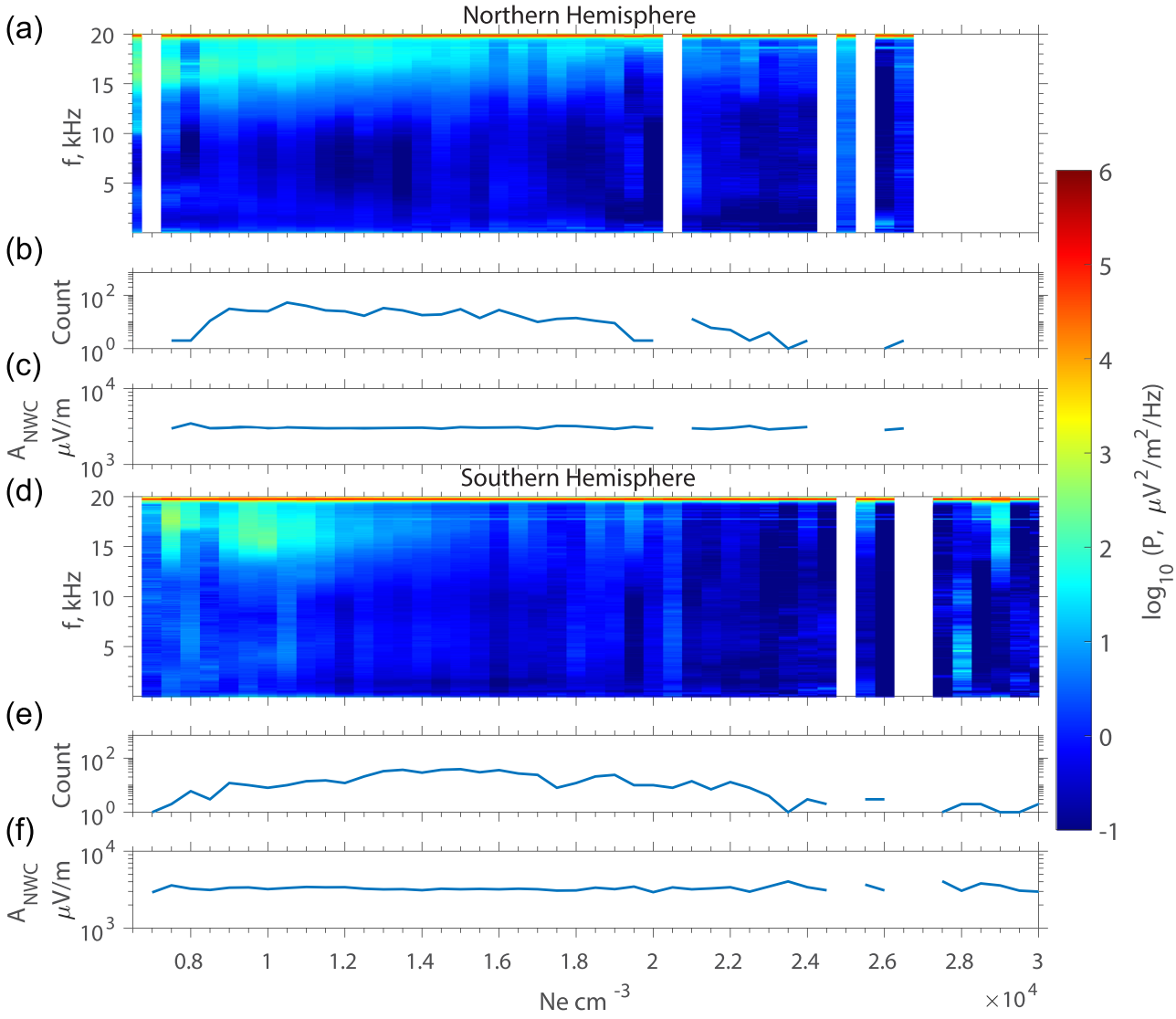

Figure 4. Panels (a) and (d) are the VLF electric wave power spectra versus frequency (*y*-axis) and plasma density (*x*-axis) at nightside in the northern and southern hemispheres, respectively. Panels (b) and (e) are the corresponding numbers of spectra in each density bins. Panels (c) and (f) are the corresponding mean NWC amplitude in each density bins.

To check the reliability of our statistical results on the effects of the NWC amplitude and the electron density, we perform an occurrence analysis of the spectral broadening. Among the spectra with the presence of NWC transmitter signals (Figure 3), we first identify the spectra of the spectral broadening signature using the criterion that power spectral density is sufficiently high (>10(μV/m)^2/Hz) for at least 100 frequency channels (about a width of 2 kHz) among the 512 frequency channels from 10 to 20 kHz. These obtained broadened spectra are sorted into bins with different values of electron density and NWC amplitude. Figure 5a shows the distribution of the number of broadened spectra (bins with sample number less than 5 are marked as blank), and Figure 5b shows the corresponding occurrence rate (the ratio between the number of the broadened spectra to the number of the spectra with the presence of NWC transmitter signals). One can see increasing occurrence rate (approaching 1) at larger A_{NWC} and smaller electron density, which supports the hypothesis that larger NWC amplitude and smaller electron density are favorable conditions for the spectral broadening. In addition, the threshold values of NWC amplitude to excite spectral broadening tend to be lower when electron density is smaller. The fitted threshold curve, $\left(\frac{A_{NWC}}{\mu V/m}\right)^{2.53}$

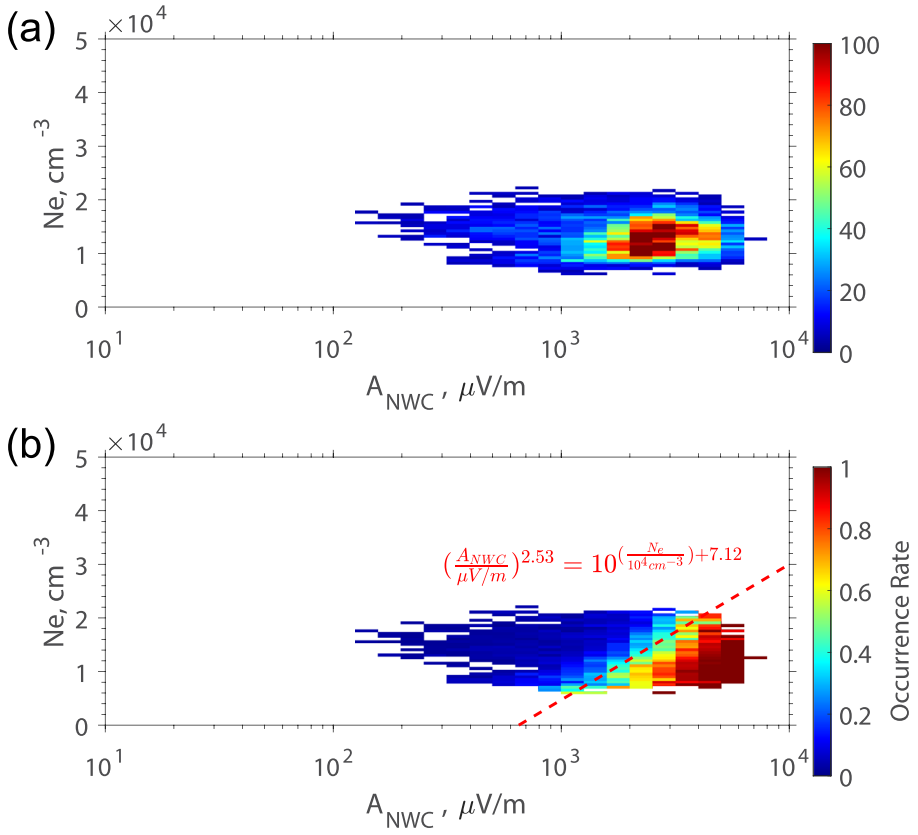

Figure 5. Panel (a) is the distribution of the number of occurrence with broadening spectra versus plasma density (*y*-axis) and NWC transmitter wave amplitude (*x*-axis). Panel (b) is the distribution of the spectral broadening occurrence rate.

$=10^{\left(\frac{Ne}{10^4 cm^{-3}}\right)+7.12}$, is obtained based on the occurrence rate of 50% in Figure 5b. The threshold values range from $\sim 10^3 \mu$V/m for electron density of 1×10^4 cm^{-3} to $\sim 10^{3.5} \mu$V/m for electron density of 2×10^4 cm^{-3}.

5. Conclusions and Discussion

In this study, we use about 6 years of observation of the DEMETER satellite to study the preferred condition for the spectral broadening of NWC transmitter emissions in the ionosphere and the statistical characteristics of the broadened VLF spectra. The dependences of the spectral broadening on the NWC amplitude and the background plasma density are examined, and the threshold for the NWC amplitude is obtained. The main conclusions are summarized below:

1. The broadened emissions of NWC VLF transmitter signals are mainly electrostatic and occur at both the source (southern) and conjugate (northern) hemispheres, in both VLF and HF frequency bands, but their occurrences are preferred at nightside than dayside.
2. The spectral broadening occurs with a critical NWC signal amplitude of about $10^{3.4}$ μV/m. The intensity and frequency width of the broadened VLF spectra increase as the NWC amplitude increases.
3. When spectral broadening occurs, the intensity and frequency width of the broadened VLF spectra increase as the background electron density decreases.

Here we discuss the dependencies of the spectral broadening and compare with the theories of three possible plasma instabilities put forth in Mishin et al. (2010) to explain the spectral broadening. The three plasma instabilities (PI) includes (1) nonresonant decay via nonlinear Landau damping on electrons (PI_{nl}), (2) resonant decay into lower hybrid and ion Bernstein modes (PI_{ib}), and (3) a purely growing (PI_{pg}) mode when the Stokes and anti-Stokes sidebands couple with density irregularities. The threshold values (equations 1–3) and the growth rates (equations 4–6) were provided in Mishin et al. (2010) for the three instabilities,

respectively. We would like to note the following few points. First, the growth rates of all the three instabilities increase as the amplitude of NWC transmitter increases, which is supported by our statistical result that the intensity and frequency width of the spectral broadening increase as the amplitude of NWC transmitter increases. Second, Mishin et al.'s (2010) analysis suggests that the PI_{nl} should be the primary instability at $f \geq f_{lhr}$ based on the comparison of growth rates for the three instabilities. Thus, for the effect of the plasma density, we check the variations of the instability threshold and growth rate of PI_{nl} versus different density values by using the corresponding formulas (equations 1 and 4 in Mishin et al., 2010). According to equations 1 and 4 in Mishin et al. (2010), as the density increases, the instability threshold increases, and the growth rate also increases with the density. While the growth rate decrease due to decreasing electron density might lead to a longer time scale of the spectral broadening, the lowering of the instability threshold due to decreasing electron density explains higher occurrence of spectral broadening. In addition, the threshold value of 1–3 mV/m (Figure 5b), depending on the value of plasma density, is consistent with the theoretical threshold values predicted by the PI_{nl} (the top panel of Figure 2 in Mishin et al., 2010). Another possible factor is that as plasma density decreases, f_{lhr} decreases, which tends to increase the frequency width of the broadened VLF emission. However, this effect of plasma density on the f_{lhr} is not quite significant when the electron plasma frequency is much larger than the electron cyclotron frequency. The ion composition may play a role on the f_{lhr} and thus the spectral broadening, which is left as further study.

The obtained dependencies and thresholds of the spectral broadening phenomenon due to NWC transmitter signals are valuable for understanding the underlying mechanism. These results can help guide numerical models (particle in cell simulation) in producing the broadened spectra and make a direct comparison with simulation results, which are left as future work.

Data Availability Statement

The DEMETER data shown in the paper can be downloaded from https://cdpp-archive.cnes.fr/.

Acknowledgments

Work at UTD was supported by the NSF Grant 1702805 through the Geospace Environment Modeling program and the AFOSR Grant FA9550-16-1-0344. This study is related to data recorded by the microsatellite DEMETER, which was operated thanks to the French Centre National d'Etudes Spatiales (CNES). We also thank J.J. Berthelier and J.P. Lebreton, the PIs of ICE and ISL, respectively.

References

Bell, T. F., Graf, K., Inan, U. S., Piddyachiy, D., & Parrot, M. (2011). DEMETER observations of ionospheric heating by powerful VLF transmitters. *Geophysical Research Letters*, *38*, L11103. https://doi.org/10.1029/2011GL047503

Berthelier, J., Godefroy, M., Leblanc, F., Malingre, M., Menvielle, M., Lagoutte, D., et al. (2006a). ICE, the electric field experiment on DEMETER. First results of the DEMETER micro-satellite. *Planetary and Space Science*, *54*(5), 456–471. https://doi.org/10.1016/j.pss.2005.10.016

Berthelier, J. J., Godefroy, M., Leblanc, F., Malingre, M., Menvielle, M., Lagoutte, D., et al. (2006b). ICE, the electric field experiment on DEMETER. *Planetary and Space Science*, *54*(5), 456–471. https://doi.org/10.1016/j.pss.2005.10.016

Berthelier, J.-J., Malingre, M., Pfaff, R., Seran, E., Pottelette, R., Jasperse, J., et al. (2008). Lightning-induced plasma turbulence and ion heating in equatorial ionospheric depletions. *Nature Geoscience*, *1*(2), 101–105. https://doi.org/10.1038/ngeo109

Galinsky, V. L., Shevchenko, V. I., Mishin, E. V., & Starks, M. J. (2011). Numerical modeling of 3D weak turbulence driven by high-power VLF pump waves in the topside ionosphere. *Geophysical Research Letters*, *38*, L16105. https://doi.org/10.1029/2011GL048441

Gamble, R. J., Rodger, C. J., Clilverd, M. A., Sauvaud, J.-A., Thomson, N. R., Stewart, S. L., et al. (2008). Radiation belt electron precipitation by man-made VLF transmissions. *Journal of Geophysical Research*, *113*, A10211. https://doi.org/10.1029/2008JA013369

Graf, K. L., Inan, U. S., Piddyachiy, D., Kulkarni, P., Parrot, M., & Sauvaud, J. A. (2009). DEMETER observations of transmitter-induced precipitation of inner radiation belt electrons. *Journal of Geophysical Research*, *114*, A07205. https://doi.org/10.1029/2008JA013949

Inan, U. S., Golkowski, M., Casey, M. K., Moore, R. C., Peter, W., Kulkarni, P., et al. (2007). Subionospheric VLF observations of transmitter-induced precipitation of inner radiation belt electrons. *Geophysical Research Letters*, *34*, L02106. https://doi.org/10.1029/2006GL028494

Lebreton, J.-P., Stverak, S., Travnicek, P., Maksimovic, M., Klinge, D., Merikallio, S., et al. (2006). The ISL Langmuir probe experiment processing onboard DEMETER: Scientific objectives, description and first results. First results of the DEMETER micro-satellite. *Planetary and Space Science*, *54*(5), 472–486. https://doi.org/10.1016/j.pss.2005.10.017

Li, X., Ma, Y., Wang, P., Lu, H., Zhang, X., Huang, J., et al. (2012). Study of the North West Cape electron belts observed by DEMETER satellite. *Journal of Geophysical Research*, *117*, A04201. https://doi.org/10.1029/2011JA017121

Marshall, R. A., Newsome, R. T., Lehtinen, N. G., Lavassar, N., & Inan, U. S. (2010). Optical signatures of radiation belt electron precipitation induced by ground-based VLF transmitters. *Journal of Geophysical Research*, *115*, A08206. https://doi.org/10.1029/2010JA015394

Mishin, E. V., Starks, M. J., Ginet, G. P., & Quinn, R. A. (2010). Nonlinear VLF effects in the topside ionosphere. *Geophysical Research Letters*, *37*, L04101. https://doi.org/10.1029/2009GL042010

Parrot, M., Benoist, D., Berthelier, J., Blecki, J., Chapuis, Y., Colin, F., et al. (2006). The magnetic field experiment IMSC and its data processing onboard DEMETER: Scientific objectives, description and first results. *Planetary and Space Science*, *54*(5), 441–455. https://doi.org/10.1016/j.pss.2005.10.015

Parrot, M., Inan, U. S., Lehtinen, N. G., & Pinçon, J. L. (2009). Penetration of lightning MF signals to the upper ionosphere over VLF ground-based transmitters. *Journal of Geophysical Research*, *114*, A12318. https://doi.org/10.1029/2009JA014598

Parrot, M., Sauvaud, J. A., Berthelier, J. J., & Lebreton, J. P. (2007). First in-situ observations of strong ionospheric perturbations generated by a powerful VLF ground-based transmitter. *Geophysical Research Letters*, *34*, L11111. https://doi.org/10.1029/2007GL029368

Riggin, D., & Kelley, M. C. (1982). The possible production of lower hybrid parametric instabilities by VLF ground transmitters and by natural emissions. *Journal of Geophysical Research*, *87*(A4), 2545–2548. https://doi.org/10.1029/JA087iA04p02545

Sauvaud, J.-A., Maggiolo, R., Jacquey, C., Parrot, M., Berthelier, J.-J., Gamble, R. J., & Rodger, C. J. (2008). Radiation belt electron precipitation due to VLF transmitters: Satellite observations. *Geophysical Research Letters*, *35*, L09101. https://doi.org/10.1029/2008GL033194

Zhang, Z., Chen, L., Li, X., Xia, Z., Heelis, R. A., & Horne, R. B. (2018). Observed propagation route of VLF transmitter signals in the magnetosphere. *Journal of Geophysical Research: Space Physics*, *123*, 5528–5537. https://doi.org/10.1029/2018JA025637